AIAA JOURNAL
Vol. 47, No. 5, May 2009

Suppression of Cavity Loads Using Leading-Edge Blowing

Srinivasan Arunajatesan, Chandrasekhar Kannepalli, and Neeraj Sinha
Combustion Research and Flow Technology, Inc., Pipersville, Pennsylvania 18947
Michael Sheehan and Farrukh Alvi
Florida A & M and Florida State University, Tallahassee, Florida 32310
and
George Shumway* and Lawrence Ukeiley*
University of Florida, Shalimar, Florida 32579

DOI: 10.2514/1.38211

We present hybrid Reynolds-averaged Navier–Stokes/large eddy simulation-based analysis of the suppression of fluctuating pressure loads on the walls of a complex nonrectangular cavity using leading-edge mass blowing. The unique aspect of the concepts discussed here is the very low mass flow rates used to achieve significant suppression. The simulation results are used to gain insight into the mechanism governing the effectiveness of these jets. The jets are applied to an $L/D = 5.6$ cavity at supersonic conditions of Mach 1.5. The simulation results show excellent agreement with experiments demonstrating an overall reduction in fluctuating pressure levels on the order of 50% with the control concepts. The primary mechanism of reduction is the break up of the spanwise coherence in the shear layer into smaller vortical structures thus reducing the shear layer flapping and leading to a smaller imprint on the wall pressures.

Nomenclature

C_μ	=	momentum coefficient
f_m	=	frequency of mth Rossiter mode
L	=	cavity length
m	=	mode number
m_j	=	mass flow rate of jet
M_∞	=	freestream Mach number
N	=	number of jets
Q	=	freestream dynamic pressure
St_m	=	Strouhal number of mth Rossiter mode
U_j	=	jet velocity
$U_{\max}$	=	maximum velocity at station
$U_{\min}$	=	minimum velocity at station
U_∞	=	reference velocity
w	=	width of cavity leading edge
α, K	=	modified Rossiter formula constants
δ	=	thickness of upstream boundary layer
δ_w	=	vorticity thickness
$\frac{\partial u}{\partial y}\|_{\max}$	=	maximum velocity gradient at station
ρ_∞	=	reference density

I. Introduction

EXTERNAL weapons' carriages can be responsible for as much as 30% of the total vehicle drag and lead to prohibitive increases in radar signatures of current generation combat aircraft [1]. Motivated by these considerations, recent military aircraft programs have incorporated internal weapons' carriage systems. However, an internal aircraft weapons bay, when exposed to freestream flow, experiences an intense aeroacoustic environment in and around the bay [2] with unsteady pressure fluctuations as high as 160 to 180 dB. Similar cavity oscillations due to nonlinear instability wave interactions are also present in wheel wells and sensor bays in a high-speed environment. High-fluctuating pressure loads can significantly reduce the life of aerostructures in the bay and can damage sensitive electronic components. Aircraft design engineers are being challenged to develop innovative suppression methods to control the environment in the weapons bay associated with the large fluctuating pressures.

Over the years, aircraft structural design engineers have tested varied passive suppression concepts for effectiveness in attenuation of dynamic loads within the bay, for example, a small spoiler located upstream of the cavity [3], other leading- and trailing-edge devices [4], porous spoilers, [5], a small fence [6], an oscillating flap [7], etc. Passive control methods are inexpensive, simple, and, at certain flow conditions, very effective in suppressing the cavity oscillations. However, the performance of the suppression device at off-design or during time-dependent conditions (maneuvering aircraft) can degrade significantly and cavity loads might be higher than without control. Active control methods, although more complex, have the potential of adapting to differing flow conditions and, thus, can provide suppression of oscillations over the full flight spectrum. Mass injection at the leading edge of the cavity offers great potential to achieve this.

Over the past few years, several studies have been carried out (see Cattafesta et al. [8] and Rowley and Williams [9] for recent reviews) to examine the use of leading-edge mass blowing concepts to suppress the dynamic loads on the surfaces of cavities. Several of these concepts have demonstrated success, suppressing the loads by over 10 dB in many cases. However, most of these mass blowing concepts have involved the use of significant amounts of mass flow rates, rendering them impractical for full-scale applications. More recently, Zhuang et al. [10,11] and the authors and their collaborators [12–14] have demonstrated the use of low mass flow rate blowing concepts for control of cavity loads. These works have demonstrated suppression exceeding that achieved by currently deployed spoiler-type configurations. In addition, this success has been repeated at several scales and shown to have a positive effect on store separation [15], thus, rendering them very attractive in comparison to spoiler-type devices. In the present paper we examine the physical mechanisms underlying the successful suppression achieved by the use of such leading-edge blowing devices. We focus on the low supersonic regime, and all the cases in the present paper have been carried out at Mach number 1.5.

The paper is organized as follows: in Sec. II we first describe the flow configuration and simulation setup. A brief description of the

Presented as Paper 0044 at the 46th Aerospace Sciences Meeting and Exhibit, Reno, NV, 7–10 January 2008; received 22 April 2008; revision received 2 September 2008; accepted for publication 6 August 2008.

*Department of Mechanical and Aerospace Engineering, Research and Engineering Education Facility.

numerical method and turbulence model used is presented in Sec. III. Section IV presents a discussion of the wall pressure fluctuation and flowfield results from simulations of the baseline and controlled cavity cases. A discussion of the application of the proper orthogonal decomposition (POD) to the velocity field was conducted to identify the mechanism/effect of control on the structure of turbulence is also presented in this section.

II. Flow Configuration and Simulation Setup

The configuration analyzed in this work has a highly complicated geometry (Fig. 1) with strong 3-D features. A sloping floor in the front section of the cavity results in a varying depth of the cavity, and slanted sidewalls cause variations in the width. It is exactly representative of the bay studied experimentally by Ukeiley et al. [13]. The cavity length is $L = 61$ mm, its maximum width is $W = 20$ mm, and maximum depth $D = 11$ mm at the aft wall results in $L/D = 5.5$ and $L/W = 3$. Based on the classical classification of cavities this would be considered to be a open cavity [16].

In the program under which most of the work presented here was carried out, several control configurations at several scales were studied, mostly under supersonic conditions. For the cases presented here, the flow conditions are representative of the cases presented in [13], which were examined at the National Center for Physical Acoustics (NCPA) at the University of Mississippi and the Advanced Aero-Propulsion Laboratory (AAPL) at the Florida A&M University and Florida State University College of Engineering. The freestream Mach number is 1.5, and the upstream boundary layer for this case is $\delta/D = 0.15$, which is close to the boundary-layer thickness in the NCPA tunnel facility. The dynamic pressure ($\mathbf{Q} = 1/2\rho_\infty U_\infty^2$) for the cases modeled here was 9.41 psi.

Three different suppression concepts are analyzed here (schematics of the concepts are shown in Fig. 2). These consist of:

1) *A "1δ" spoiler*: This consists of a fence of height equal to one boundary layer height located at the leading edge of the cavity. The thickness of the spoiler (dimension in the streamwise direction) is equal to its height. The spoiler is mounted so that its aft wall is flush with the front wall of the cavity. In the spanwise direction the spoiler only spans the width of the leading edge of the cavity.

2) *Microjets*: In this concept, eight 400 μm microjets are located just upstream of the cavity leading edge at a distance of four microjet diameters from the leading edge. The spacing between the microjets matches that in the experimental work at AAPL presented in [13,14], which was parametrically optimized. The microjet pressures are 40 psig and are operated choked. These conditions correspond to the conditions where the microjets' effectiveness started to saturate.

3) *Slotted Jets*: In this concept, a set of three slots spanning the leading edge of the cavity are located 1.6 mm upstream of the cavity leading edge. The slots are 0.254 mm wide in the streamwise direction, the spanwise width (1.47 mm) of the slots correspond to the slot 4 configuration in Ukeiley et al. [13]. The operating pressures for this configuration are set at 20 psi, and the slots are also choked.

It is worth noting that the preceding configurations and corresponding conditions were found to be the most effective among the many variations that were experimentally tested. Details of the configuration and conditions that were tested were discussed in Ukeiley et al. [13]. It is further worth noting that both of the injectors being studied here were optimized in terms of their geometries yet the spoiler was not, hence any comparison between the these cases should be evaluated carefully. Analogous to the analysis presented in [13], the jet blowing can also be expressed in terms of a momentum coefficient defined as follows:

$$C_\mu = \frac{Nm_j U_j}{1/2\rho_\infty U_\infty^2 w\delta} \tag{1}$$

For the microjets C_μ is 0.25, and for the slotted jets it is 0.056. This definition relates the momentum of the control jet to the momentum in the boundary layer upstream of the cavity leading edge. Therefore, C_μ is the ratio of the steady momentum flux issuing from the actuators to that of the base flowfield being examined and/or controlled. To define a flux for the freestream, an appropriate area must be chosen that captures the essential length scales of the problem. In the present case, a boundary-layer integral length (height in this case) is the obvious choice for the length scale associated with the incoming boundary layer/cavity shear layer. We chose the boundary-layer thickness as it is the one most commonly used in defining the effect of actuators in active flow control problems and has been used by some of the present authors [13]. Alternatively, one may use a different integral scale such as momentum thickness; however, this would simply modify C_μ by a fixed constant.

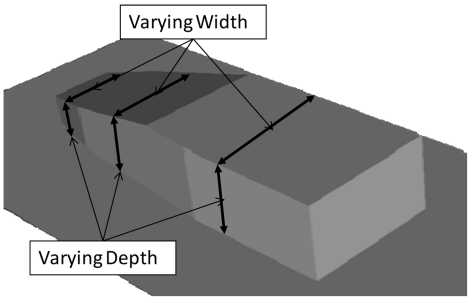

Fig. 1 Schematic of the nonrectangular cavity being studied in the present work.

III. Numerical Method and RANS-LES Modeling

All the numerical simulations in the present effort were carried out using CRAFT Tech's CRAFT CFD® software. For LES (large eddy simulation) and RANS-LES (Reynolds-averaged Navier–Stokes/large eddy simulation) applications, the CRAFT CFD® is implemented with an upwind-biased, Roe-flux-extrapolation procedure that has been extended to fifth order [17,18] for the inviscid and fourth-order central differencing for the viscous terms. This scheme has been shown to be capable of accurately capturing vortex transport with minimal dissipation. Temporally, the code includes both an explicit fourth-order Runga–Kutta scheme and a second-order three-factor approximate factorization (AF) implicit scheme. For the studies described here, the implicit scheme was used. For subgrid modeling, the code includes a compressible version of the algebraic Smagorinsky model as well as a one-equation model [19]. The hybrid RANS-LES model uses the standard k-ε equations.

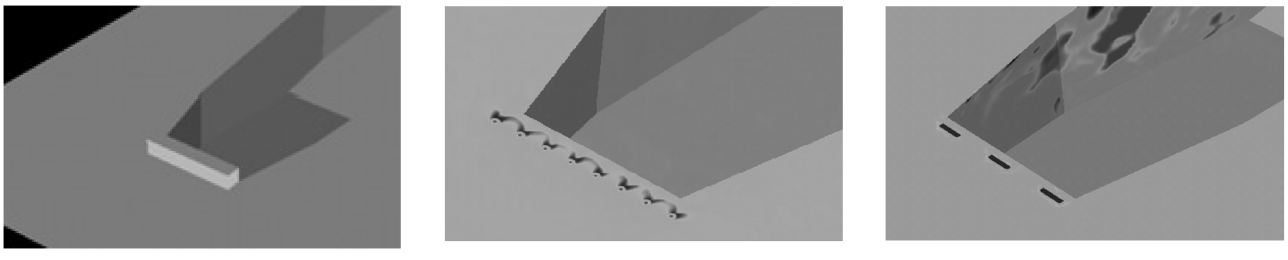

a) Schematic of the fence spoiler **b) Schematic of the microjets** **c) Schematic of the slot jets**

Fig. 2 Schematic of the control configurations studied in this paper.

The eddy viscosity is suitably scaled down in LES regions based on an assessment of the local resolution levels and the local range of scales that this resolution would permit. Details of this model can be found in [20].

In the experiments that the simulations are based on, the cavities were mounted on the tunnel roof, and care was taken to ensure that no reflections from the tunnel floor affected the cavity flowfield. In the simulations, the tunnel floor is not modeled, instead nonreflective far-field boundary conditions are imposed on that boundary. The boundary conditions for the tunnel roof and cavity walls use no-slip adiabatic conditions. For the upstream boundary conditions, the boundary layer has been determined from a RANS simulation of the nozzle and is imposed at the domain inlet boundary to the hybrid RANS-LES simulations of the cavity. This method of providing inflow boundary conditions has been demonstrated to be a viable and accurate method in earlier simulations of the cavities [12] and backward-facing step flows [21]. The upstream boundary is located about one cavity (aft) depth upstream of the leading edge and the downstream boundary is located about two cavity depths downstream of the cavity aft end.

IV. Results and Analysis

In this section, we present the major results from this study and compare and analyze the effects of the control concepts on the cavity flowfield. Comparisons of the effect of the control on the wall pressures are presented first along with comparisons to some of the experimental values determined from the efforts mentioned previously. Next, a discussion of the flowfield characteristics that contribute to these changes along with an analysis of the POD modes to specifically examine the changes to the dominant flow features from the application of the fluidic blowing will be presented.

The analysis presented here used data sampled from the simulations over several periods of the dominant mode of oscillations. The unsteady wall pressure data was collected over 0.06 s, which corresponds to 120 periods of the first Rossiter mode for the cavity based on its length. The power spectral density functions for the wall pressure signals were computed similar to Nichols [22] using 128 overlapping ensembles with an overlap of 66.67% and frequency resolution of 50 Hz. The flowfield statistics and snapshot POD analysis were carried out on unsteady flowfield data stored every 0.1 ms over 0.1 s of simulation.

A. Cavity Wall Pressures

The mean pressure profile along the cavity centerline is shown in Fig. 3a. The behavior of this cavity mimics classical deep cavity behavior, a more-or-less uniform floor pressure with a sharp increase at the aft end. This is in agreement with the mean pressure distribution for open cavities [23]. In addition, the mean flowfield (discussed in Sec. IV.B) shows the presence of one large recirculation bubble filling the cavity. These features justify the classification of this cavity as a open cavity.

The wall pressure spectra from the baseline case for the 3-D cavity is shown in Fig. 3b. Here, the spectra at three different points on the walls, two on the floor and one on the aft wall, 0.25D into the cavity, are shown. Also shown in the same figure are vertical lines corresponding to the Rossiter mode frequencies. The modes here are calculated using the modified Rossiter formula due to Heller and Bliss [23]

$$St_m = \frac{f_m L}{U_\infty} = \frac{m - \alpha}{[M_\infty (1 + \frac{\gamma - 1}{2} M_\infty)^{-1/2} + \frac{1}{K}]} \tag{2}$$

with constants $\alpha = 0.25$ and $K = 0.67$.

The agreement between the frequencies predicted by the numerical simulations and the semiempirical model are within 12%, which is typically found throughout the literature when these constants are used in supersonic flows.

The spectra from this highly 3-D cavity exhibit characteristics very similar to those from pressure fluctuations in a rectangular cavity. The second mode is dominant and other weaker modes close to the Rossiter mode frequencies are also seen. The characteristic length scale for these oscillations is seen to be the length of the cavity, similar to a rectangular cavity. These observations are in agreement with the characteristics observed experimentally by Ukeiley et al. [13] and Sheehan [14].

The effect of control on the wall pressures is presented in Figs. 4a–4d. Here the mean and rms pressures for the baseline and controlled cases are shown. Also shown in the rms pressure plot is a comparison with the measured data from Ukeiley et al. [13]. The imposition of control does not alter the mean pressures significantly, clearly in the figure the differences are small and the overall behavior is nearly identical. However, the effect of the control on the fluctuating pressures is quite significant for all the concepts reducing the fluctuating pressure levels. Also, from Fig. 4b–4d, the comparisons with the experimental data show that for all the cases the computed values are in reasonable agreement (within 10%) with the measured values. Although the predicted values are not in exact agreement with the measured values, the trends in the rms pressures with the imposition of control is correctly captured. The effectiveness of the slot jets and spoiler are captured very accurately, whereas the effectiveness of the microjets is slightly overpredicted. From this plot it is also seen that the mass blowing concepts perform at least as well as the spoiler or better at all the locations. The fact that the mass blowing rates can be adjusted depending upon the flow conditions means that these represent a more efficient control concept, as they can be tuned to yield consistent performance at all conditions. This is a very big limitation of a passive device such as the spoiler, which is typically optimized for a point design.

The effect of the control on the wall pressure spectra is further shown in Fig. 5. The comparisons for the slots and the microjets are

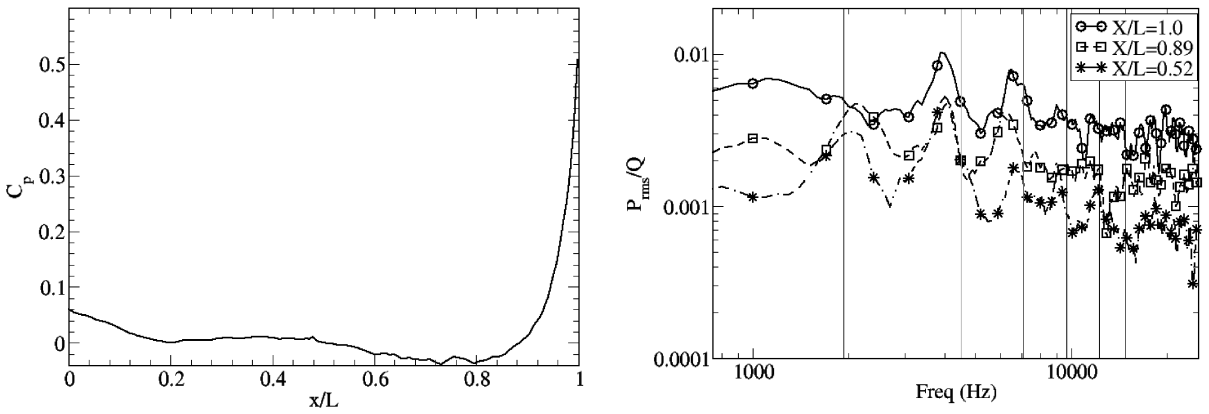

a) Mean floor pressure **b) Baseline pressure spectra**

Fig. 3 Mean pressure profile and spectra of fluctuating pressures along the cavity walls.

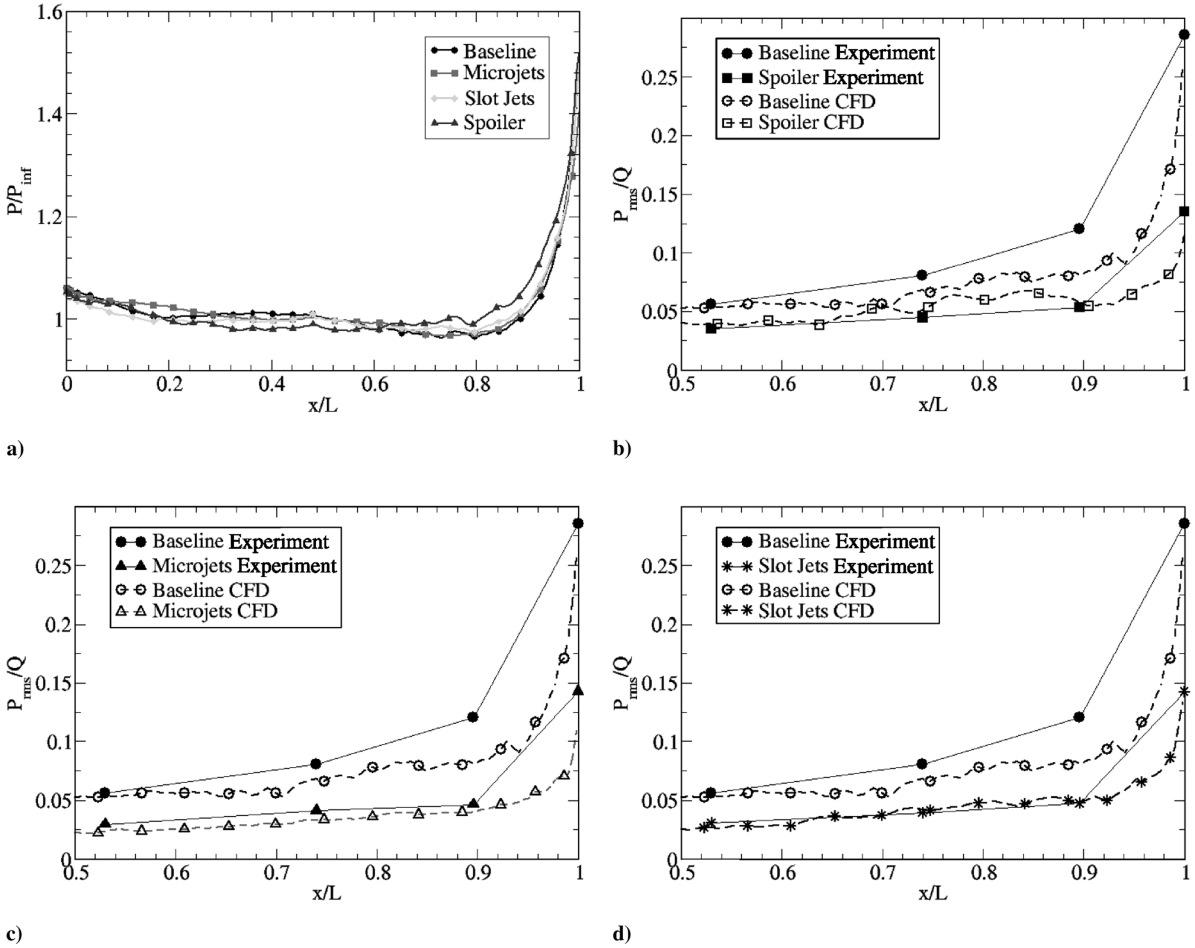

Fig. 4 Comparison of the a) mean and rms wall pressures for the baseline, b) spoiler, c) microjets, and d) slot jets controlled cavity, where CFD stands for computational fluid dynamics.

presented separately for clarity. On the aft wall pressure fluctuation levels are reduced across the entire spectrum with the dominant Rossiter mode reduced by 50% for both the cases. On the floor, the dominant second mode is not reduced significantly using microjets, whereas slot jets suppress the pressure fluctuations across the entire spectrum. These results are consistent with previous control studies [24], which demonstrated the most significant reductions on the aft wall where the fluctuating pressure levels are the highest.

B. Mean Flowfield

Comparison of mean velocity contours for the baseline, spoiler, microjets, and slot-jet cases is shown in Fig. 6, and profiles at three different locations along the length are shown in Fig. 7. All of the data plotted in these figures is along the midplane of the cavity. In Fig. 7, $y = 0$ is the lip line of the cavity, $y > 0$ is inside the cavity, and $y < 0$ corresponds to the freestream.

Compared with the baseline case, there is a strong deflection of the shear layer into the freestream by the spoiler, which is clearly visible in these figures. Because of this lofting, the shear layer impingement on the aft end of the cavity must be significantly altered. Thus, the primary source of the pressure waves inside the cavity is altered, and, hence, one would expect an alteration of the fluctuating pressure field inside the cavity. However, despite the changes to the impingement region, a stronger reverse flow velocity is seen inside the cavity. This is highlighted in the profile at the $x/L = 0.5$ location, where the magnitude of the negative streamwise velocity is greater for the spoiler case. The formation of a small, separated flow region upstream of the spoiler is seen, forming a ramp-like region. In terms of the downstream evolution, the profiles for the spoiler case are parallel to the profiles for the baseline case, implying that the lofting of the shear layer did not strongly affect its basic evolution, just shifted it. In contrast, the shear layers for the microjets and the slot jets do not show a very strong deflection relative to the baseline case. These results are consistent with that of Ukeiley et al. [24] where it was shown that lofting the shear layer alone was not sufficient to reduce the fluctuating pressure levels inside the cavity but it must include an alteration of the mean shear.

The main characteristic of the change in the mean profiles for the blowing cases is a change in the near-field shear layer thickness. This is clearly visible in the mean profile plots and is further highlighted in the vorticity thickness plot in Fig. 8. Here the vorticity thickness is defined as

$$\delta_w = \frac{U_{\max} - U_{\min}}{|\frac{\partial u}{\partial y}|_{\max}} \tag{3}$$

In the cavity, at the first location ($x/L = 0.1$), there is a slight thickening of the shear layer for both the microjet and slot jet cases. Further downstream, the thickening is visible more clearly, but, by the downstream end of the cavity, the differences vanish. The mean flow profiles near the aft end of the cavity are very close to that for the baseline case, and a slight shift is seen in the profiles, denoting a small deflection of the shear layer. This is also seen in the vorticity thickness variation with the growth rate (as measured by the slope of the vorticity thickness curve) for the microjet and slot jet cases being nearly equal to that of the baseline case, whereas the spoiler case shows an increase slope. Thus, the primary differences are confined to the upstream end of the cavity, close to the injection location.

C. Turbulent Flowfield

Shown in Figs. 9 and 10, are profiles of the normalized streamwise and normal rms velocities and the associated shear component of the Reynolds stresses close to the cavity leading edge ($x/L = 0.02, 0.1$),

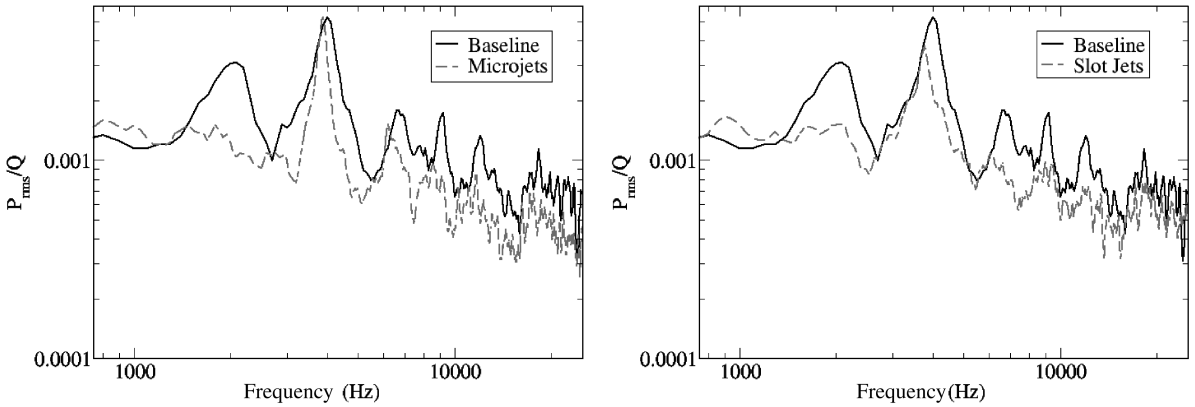

a) Microjets x/L=0.52

b) Slot jets x/L=0.52

c) Microjets aft wall

d) Slot jets aft wall

Fig. 5 Effect of slot jet and microjet control on the wall pressure spectra.

midsection ($x/L = 0.5$), and trailing edge ($x/L = 0.96$), respectively. The lofting effect of the spoiler, as discussed in terms of the mean flow, is clearly visible. The generation of shocks due to the interaction of the lofted shear layer and the freestream is also visible in the spikes in the Reynolds stress profiles. The rms velocity profiles, however, show that the overall effect on the levels or spreading rate is minimal, as the shear layer is thicker due to the lofting effect. But, the slopes in the profiles for the spoiler case are

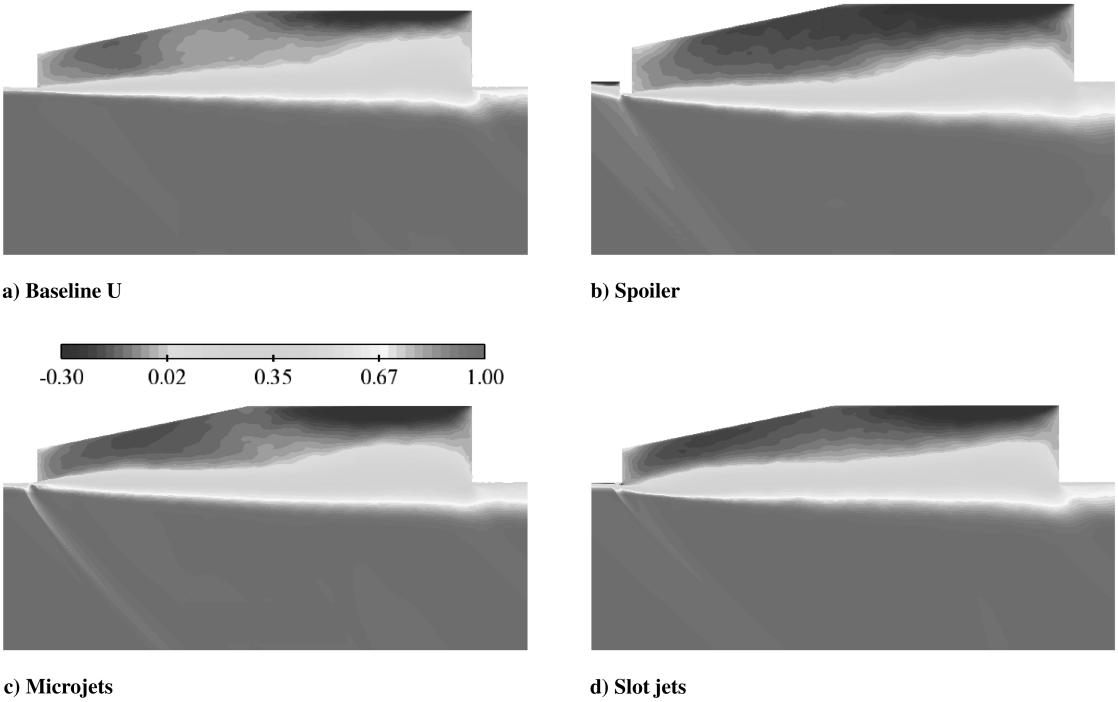

a) Baseline U

b) Spoiler

c) Microjets

d) Slot jets

Fig. 6 Mean streamwise velocity contours.

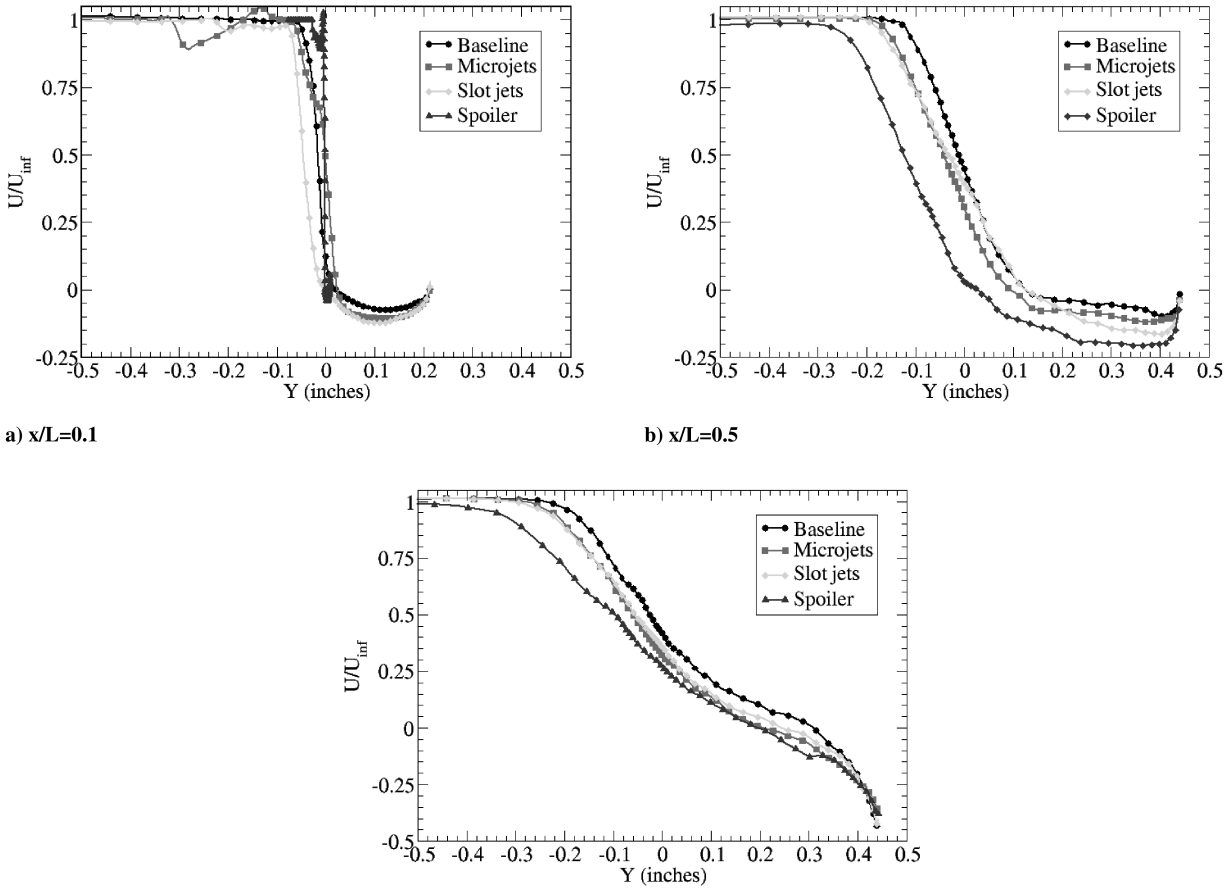

a) x/L=0.1

b) x/L=0.5

c) x/L=0.96

Fig. 7 Profiles of mean flow velocity for the concepts analyzed.

very similar to those from the baseline case and the peak magnitudes are also very close. Thus, the effect on the generation of turbulence due to the presence of the spoiler is minimal for most of the cavity length. The aft-end Reynolds stress profiles show a very different characteristic from the baseline caused by the altered interaction of the shear layer with the cavity flow due to the increased distance between the lofted shear layer and the cavity lip line.

For the mass blowing cases, we see a slightly different behavior. Here the shear layer shows an immediate thickening in the near field as evidenced by the profiles at the $x/L = 0.02$ and 0.1 locations. The intensity for the microjets is slightly higher, whereas the spreading of the shear layer is greater for the slot jet's case. The generation of the strong vortical structures reduces the spanwise coherence in the shear layer, and evidence of this is shown in Fig. 11 where contours of the streamwise velocity are shown at the axial station of $x/L = 0.1$. The shear layer in the cases with microjets is substantially more wrinkled than the baseline case with the signature of the eight microjets still visible at this station. In the case of the slot jets, the shear layer wrinkles are larger, the vortices generated by the slot jets are of the same scale as the width of the slots, and their signature is clearly visible at this station. The increased surface area between the low-speed region inside the cavity and the higher-speed flow outside for the jet blowing cases is clearly seen from these figures.

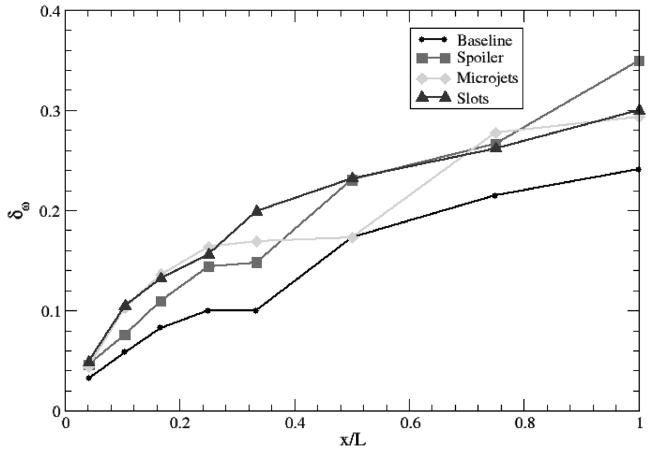

Fig. 8 Comparison of the shear layer vorticity thickness for all the cases.

The increased strain from the strong vortical structures generated by the jets increases the turbulence production levels close to the leading edge, and the addition of momentum results in a thicker shear layer. Although the thickening of the shear layer is still visible at the $x/L = 0.5$ location in the shear layer, the increased turbulence levels is not. The increased turbulence level is only visible for a short distance from the leading edge. At the aft end, the mass blowing cases show a clear thickening of the shear layer. However the difference in the turbulent stress levels is not significant at this location compared with the baseline case.

The rms profiles show differing behavior for the u and v components. The u_{rms} levels do not show very significant differences between the baseline and (jet) controlled cases. However, the v_{rms} velocities show a slight reduction in the magnitudes downstream. Using experimental PIV measurements, Sheehan [14] observed a marked reduction in the v_{rms} levels in the aft end of the cavity for the microjet controlled case. A comparison of the v_{rms} contours for baseline and microjet cases is shown in Fig. 12. The experimental data presented in [14] is also presented for comparison. It should be mentioned here that the experimental measurements were made on a cavity with constant width and only depth variations. However, on the centerline one would not expect to see significant differences due

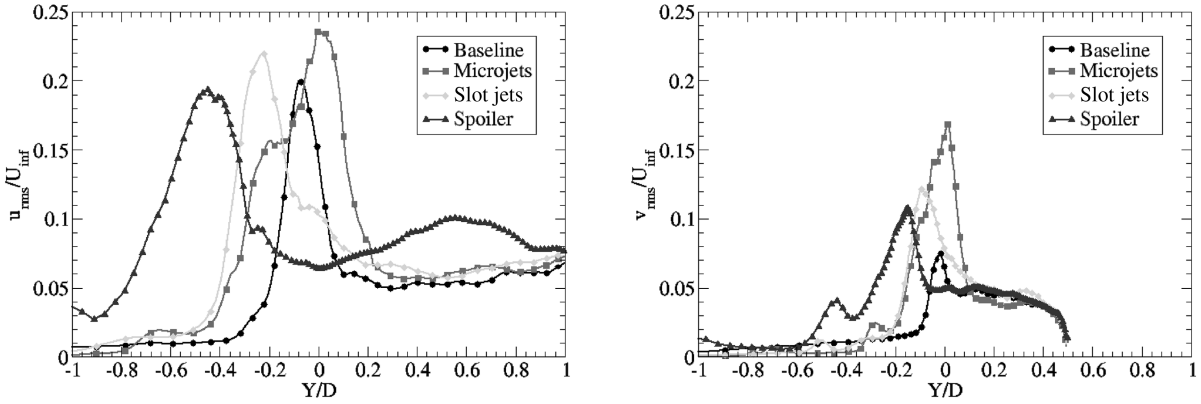

a) x/L=0.02

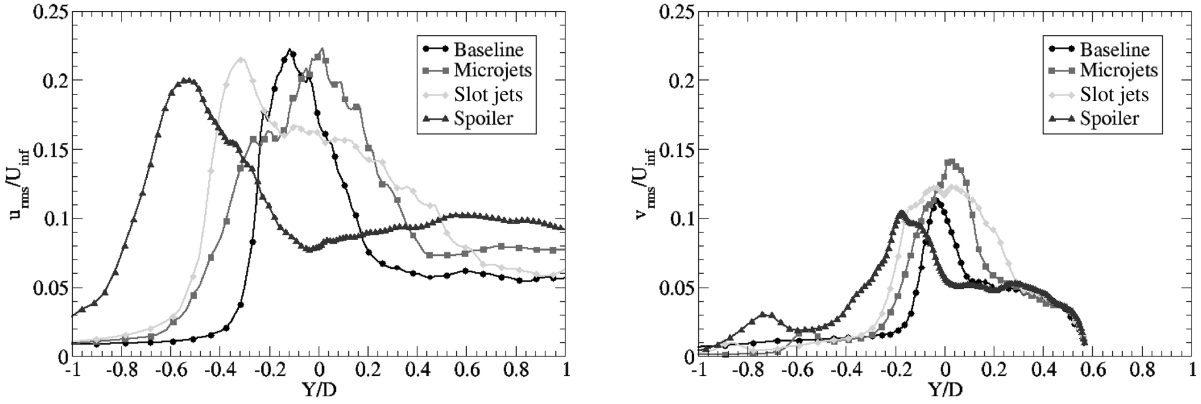

b) x/L=0.1

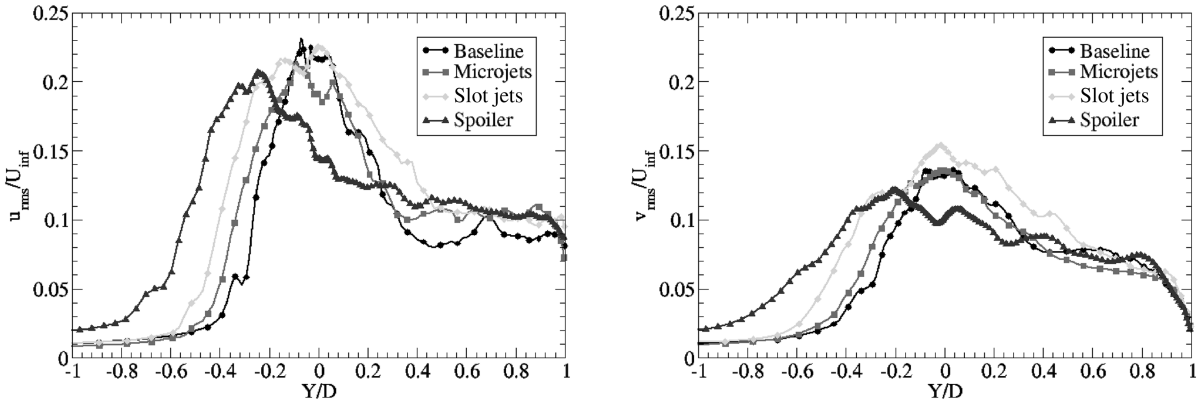

c) x/L= 0.5

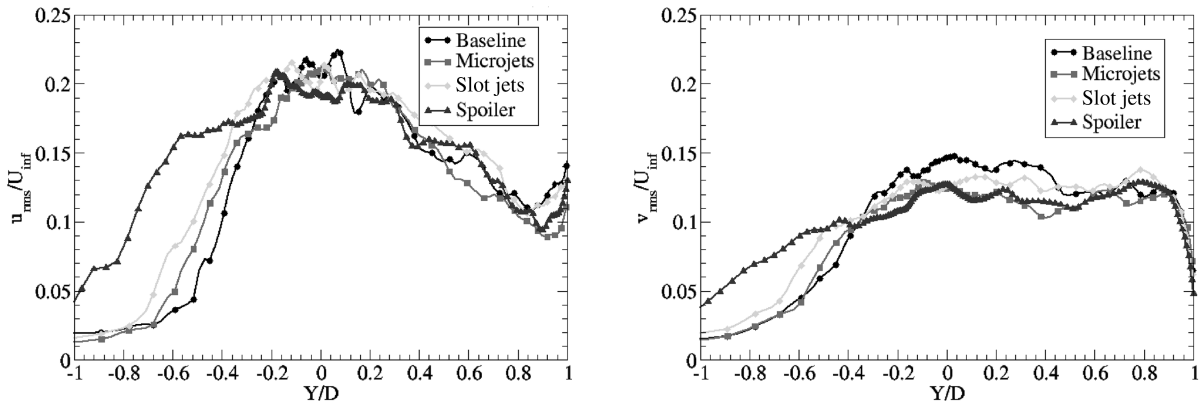

d) x/L=0.96

U_{rms} V_{rms}

Fig. 9 Comparison of profiles of *u* and *v* velocity rms for the baseline and controlled cases.

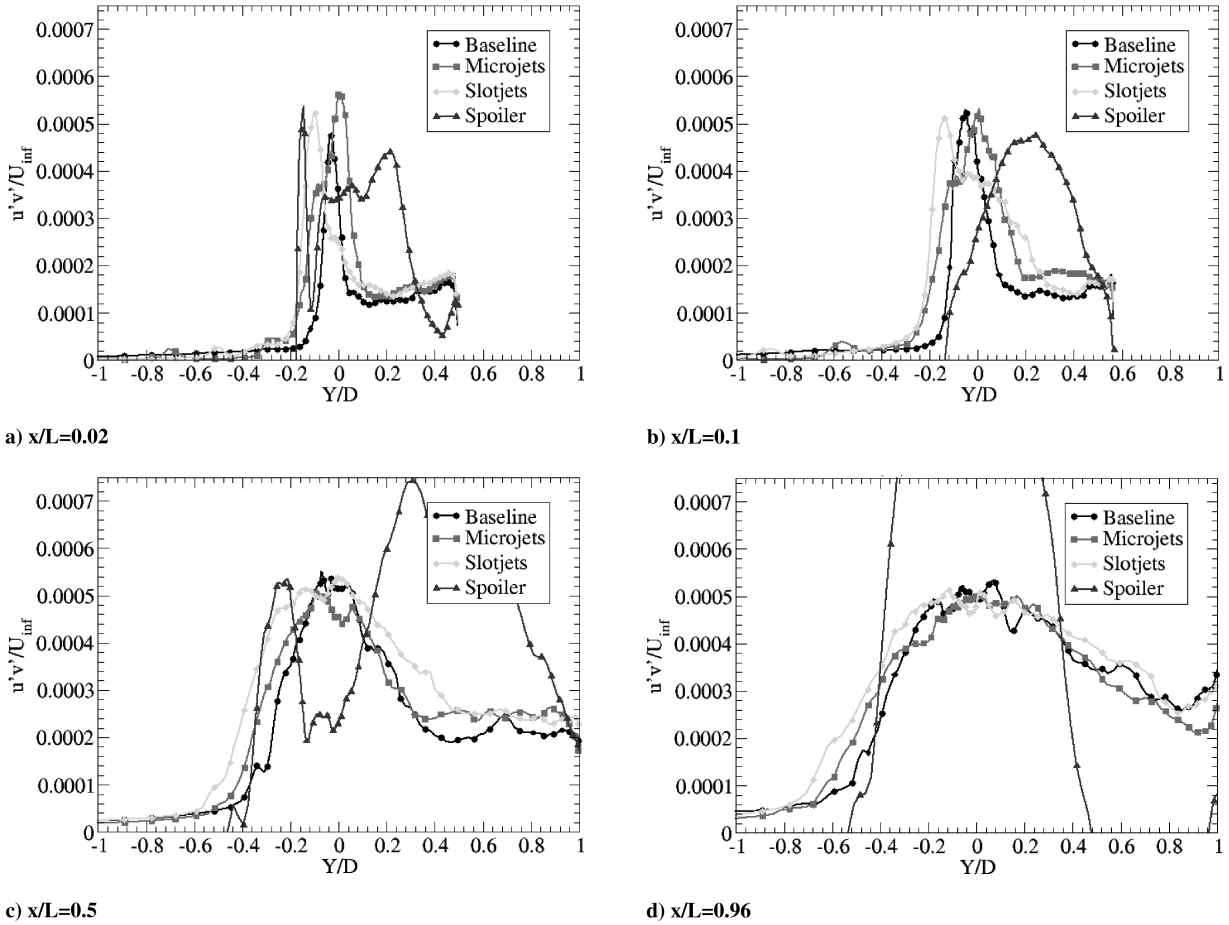

Fig. 10 Comparison of the profiles of Reynolds shear stress ($u'v'$) for the baseline and controlled cases.

to the geometry. A reduction in intensity levels and the size of the unsteady region in the aft end of the cavity is observed in the simulations, analogous to the experiments. However, the reduction observed in the experiments is more marked than that seen in the simulations. An examination of the contours from the slot jet's case (not shown here) do not show the same behavior, as the v_{rms} contours are not altered to the same extent as the microjet's case.

From the preceding results, it is clear that the control mechanism of the mass blowing concepts is significantly different from that of the spoiler. Although the spoiler effects little change in the turbulent

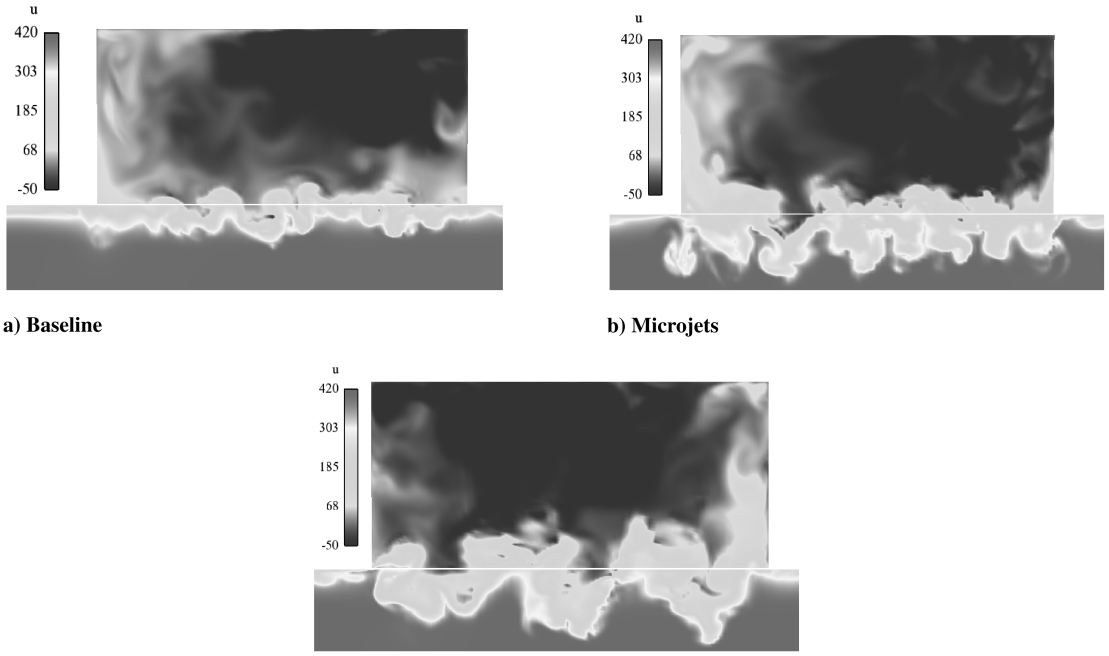

Fig. 11 Contours of instantaneous axial velocity at $x/L = 0.1$.

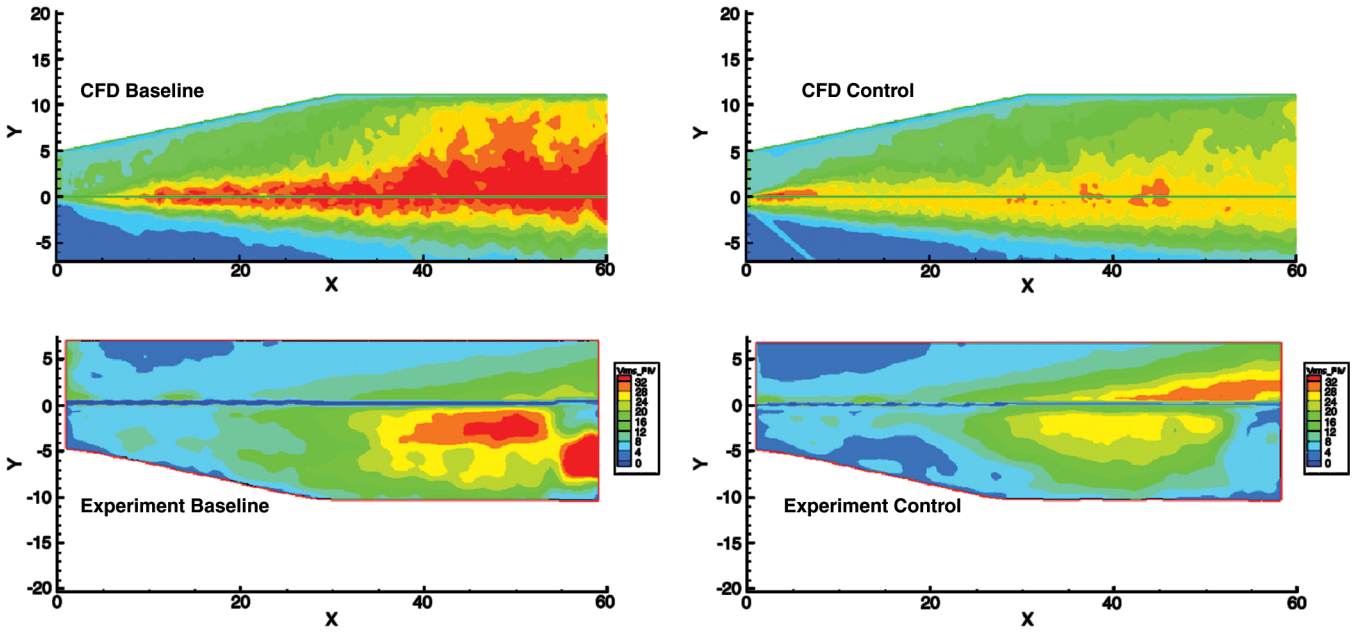

Fig. 12 V_{rms} velocity contours for the baseline and microjet cases.

flowfield evolution other than to loft the shear layer, the low mass flow rate blowing devices affect the small-scale structure of the shear layer, and, thus, affect the overall flowfield. The levels of turbulent kinetic energy and the thickness of the shear layer increase notably in the near field. There is an increase in the levels of turbulence and its production close to the jets. The increase in the kinetic energy is caused by the increase in the Reynolds stress levels in the near field. This signature of the jets lasts a short distance downstream, and the turbulence production magnitudes close to the aft end of the cavity show only small changes from that of the baseline cavity. This is likely due to the increase in the near-field turbulent kinetic energy production levels being offset by an increase in the dissipation rates further downstream resulting from the smaller-length scale structures generated by the jets. The spanwise coherence that is present in the baseline shear layer of the cavity is clearly seen to be broken down by the jets, creating smaller vortical structures and increased strain. The predominantly spanwise component of vorticity in the baseline case is reoriented and redistributed into the streamwise direction due to the generation of counter rotating streamwise vortices by the control jets. These smaller vortical structures impinging on the aft wall of the cavity will have smaller pressure fluctuations imprint on the wall. Thus, the effect of control (which is quite weak considering the small mass flow rates used) seems to significantly affect the mean and turbulence structure only close to the point of control, but this subtle yet small change in turbulence structure is enough to cause the reduction in rms of pressure levels. The levels of turbulence at the aft walls do not change much, but there is redistribution of energy probably from larger vortical structures in the baseline case to smaller structures in the controlled cases that leads to the overall reduction in the pressure levels on the cavity walls.

D. Proper Orthogonal Decomposition Analysis of Cavity Flowfields

Examination of the modes from the application of the proper orthogonal decomposition (POD) to these flowfields were carried out to further understand the effects of the control on the flow. The POD was first introduced as an unbiased mathematical method to identify coherent structures in turbulent flows by Lumley [25]. The POD modes decompose the flowfield into a basis set that optimizes the kinetic energy. These modes are the solution to a Freholm integral eigenvalue problem with the two-point velocity correlation tensor as its kernel [26]. Hence, this is a useful tool to examine the most energetic features of the flowfield. The following sections will compare the features of the dominant modes to understand the effects of the control on the turbulent structure. Results for the baseline cavity are compared with the microjet control cases, as these were the only cases where experimental flowfield data is available. The snapshot method [27] was used to extract the POD modes from the flowfield solution due to its computational efficiency with highly spatially resolved data. The analysis discussed first only uses the velocity data from the cavity midplane $z = 0$. The kinetic energy norm comprising only of u' and v' (neglecting w') is used to compare with the modes obtained from PIV on a similar plane from the experimental data [28].

Figure 13 shows the convergence of the POD modes for both the baseline and microjet case with varying numbers of flowfield snapshots used in the kernel. This plot clearly shows the number of samples used to construct the POD kernel does not affect the amount of energy in the first few modes, yet, the number of snapshots does affect the overall convergence of the energy and will require one to only discuss the results as they pertain to these modes. For the baseline case, the amount of energy in the first five modes converge with 259 snapshots, with the first mode having approximately 5% of the energy. For the control case, the amount of energy in the first five modes converge with 271 snapshots with the first mode having approximately 9% of the energy. All results will henceforth be presented for the 259- and 271-mode POD for the baseline and control cases, respectively. An interesting observation from these plots is that, contrary to expectations, the convergence of the control case is better than the baseline case (Fig. 14a). There is more energy in the first mode, which has typically been interpreted to imply an increase in large-scale organization of the flow. As has been discussed here and elsewhere [12], the use of microjets leads to a reduction in the flow structure coherence. This behavior of the modes is also observed experimentally, as shown in Fig. 14b where the POD modes for the experimental data set also show that the amount of energy in the first mode is larger for the controlled flow for the baseline even though these modes contain a higher percentage of the overall energy. However, one must be careful in interpreting these results, as it will be demonstrated later that neglecting the w' in the norm has led to this contrary result, and a full 3-D POD may be required. The effects of applying the POD to limited components of the velocity field has also been investigated in the far field of an axisymmetric jet where Wanstrom et al. [29] demonstrated that POD using one component yielded different results than that when all three were included.

A comparison of the first three POD modes of the streamwise component from the experiment discussed in [14] and simulations

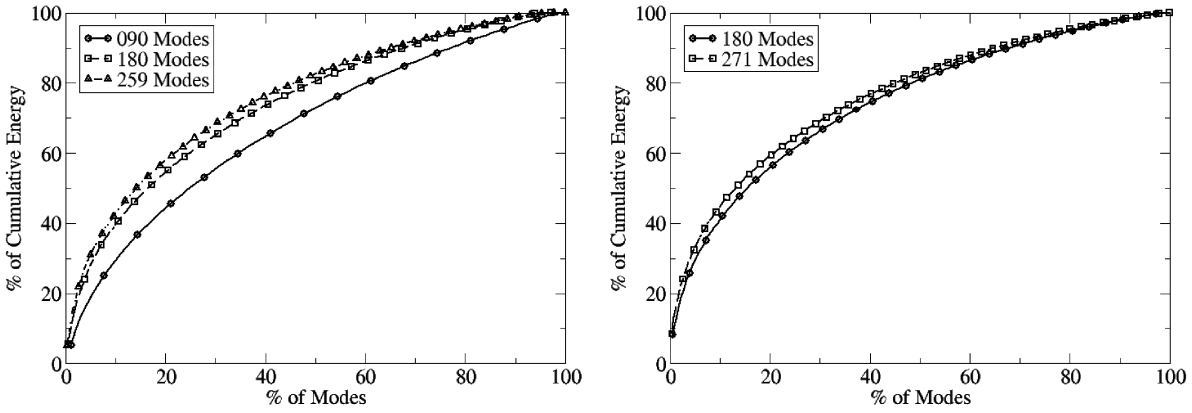

a) No control **b) With control via microjets**

Fig. 13 Convergence of POD modes for simulations.

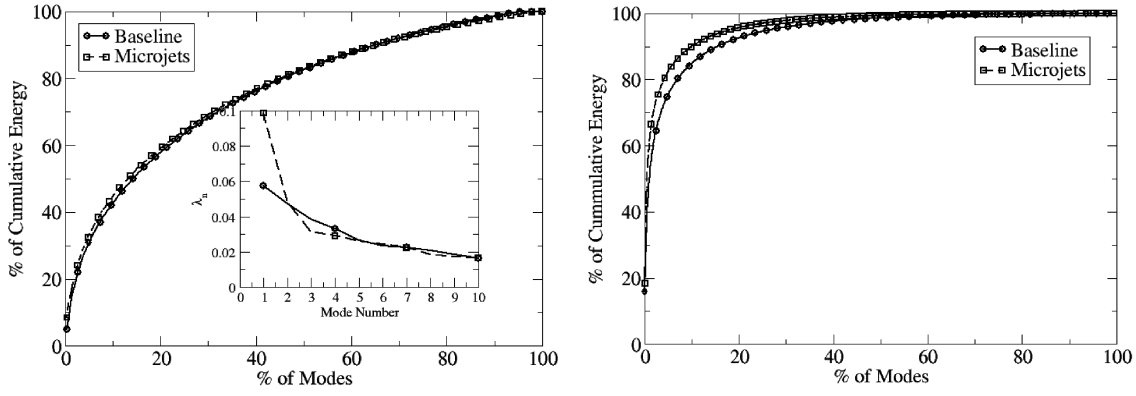

a) Simulation **b) Experiment**

Fig. 14 Convergence of POD modes with and without control.

are shown in Fig. 15. In general, the experimentally and numerically extracted POD modes show agreement with the differences in spatial resolution being quite apparent though. For the first mode the effect of control is to loft the shear layer slightly over the cavity (Fig. 15), as is shown qualitatively by both the simulation and experiment. However, the effect is more pronounced in the experiment. The second and third modes are qualitatively similar with the third mode representing the dominant wavelength of structures that is very similar to that in the experiment. Further, the modes with and without control appear to be more or less similar in nature except in the close proximity to the leading edge of the cavity where the control concept is applied. This inference reinforces the earlier results about the turbulence field being only slightly different for most of the cavity except near the leading edge.

Because the major effect of the control concepts is to reduce the rms of the pressure fluctuations, applying POD to the pressure field can be expected to yield further physical insight into the effects of control. Moreover, the pressure field has essentially a 2-D structure in the flowfield compared with the velocity field, and, thus, a 2-D application of the POD analysis (using the snapshot of the midspan plane) is more physically justified. The convergence of the pressure modes is plotted in Fig. 16 for both the baseline and control cases with the first mode in the control case being still more dominant. However, the next several modes for the baseline case contain more energy than the controlled case before the convergence plots cross back over showing a more rapid convergence in the higher modes for the controlled case. Discounting the first mode, the convergence for the control case shows that there is a less organized flow with the introduction of control and, hence, the slower convergence among the first 10 modes. The first mode of the control case, however, has more energy ($\sim$15%) when compared with the baseline first mode that has $\sim$10%. Looking at the actual magnitude of the eigenvalue (inset of Fig. 16) one can see that for the control case there is higher energy in the first mode when compared with the baseline, but in the subsequent modes the energy falls much more rapidly than in the baseline case.

The spatial distribution of the first mode of the baseline case clearly points to the fact that the most energetic feature of the flow is that impinging on the aft wall as shown in Fig. 17. Mode 2 highlights a dominant wavelength (or a tone) in the shear layer over the cavity, whereas mode 3 has a mixed component of energy in the shear layer, some in the recirculation bubble close to leading edge of the cavity and some in the impinging event on the aft wall. For the control case, however, it is very interesting to note that the most energetic part of the flowfield (mode 1) is in the separation bubble close to the cavity leading edge. Mode 2 points to a shorter wavelength and, consequently, a much higher frequency tone than the baseline case, although it is only in mode 3 that we see a distribution that is representative of the impinging event on the aft wall of the cavity. The application of control has clearly altered the organization of the energy-carrying structures. In the baseline case, it is the impinging event that is the dominant, and with control this event is reduced to a lesser/lower mode. Though not completely conclusive, this partially helps to explain the reduction in the noise levels for cavities with the microjets as a control concept.

Finally, a full 3-D POD over the whole flowfield of the cavity simulations was performed, which included the w' component in evaluating the kinetic energy norm. The energy distribution for this case is shown in Fig. 18a. The expected behavior is seen here with the baseline case showing a higher energy content in the lowest modes. The first three POD modes for the U, V, and W component of the vector field for both the baseline and control cases is shown in

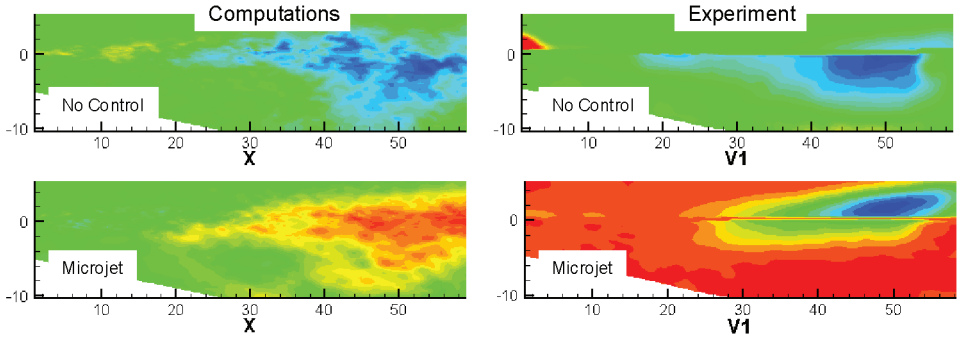

a) Mode 1

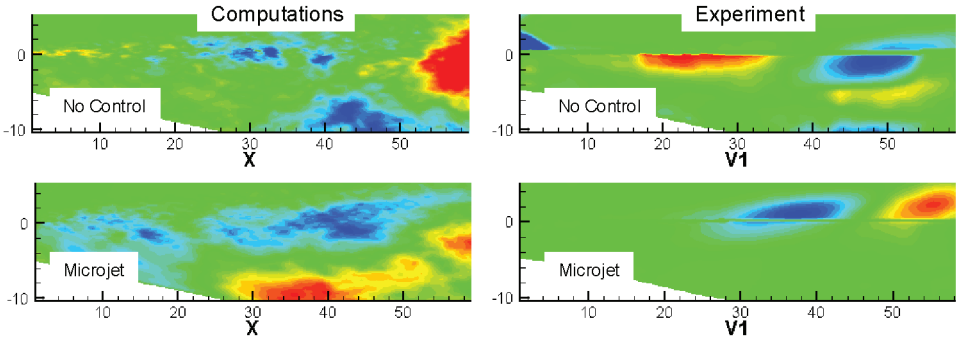

b) Mode 2

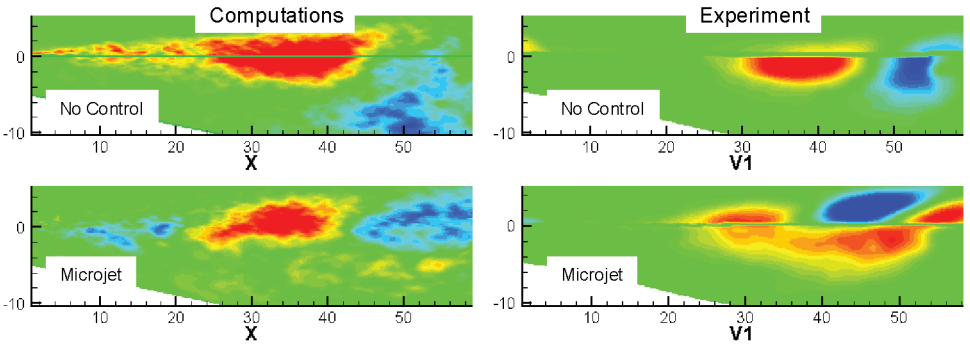

c) Mode 3

Fig. 15 Comparison of streamwise POD modes of baseline vs control cases.

Figs. 18b–18d. It is very interesting to note that the slice along the midplane of the 3-D POD modes is quite different from the 2-D modes of the velocity field. Further, for the 2-D POD, the baseline- and control-case modes looked very similar in structure (Fig. 15) but for the 3-D POD they are very different in structure. In addition, for the control case, the POD modes of the velocity now correlate quite well with the 2-D pressure modes, especially for the *U*- and *V*-velocity components. The first mode shows energy in the re-circulation bubble close to the leading edge of the cavity, the second mode highlights the energy of the shear layer toward the aft end of the cavity, and only in the third mode do we see energy associated with the impinging event on the aft wall. These results clearly

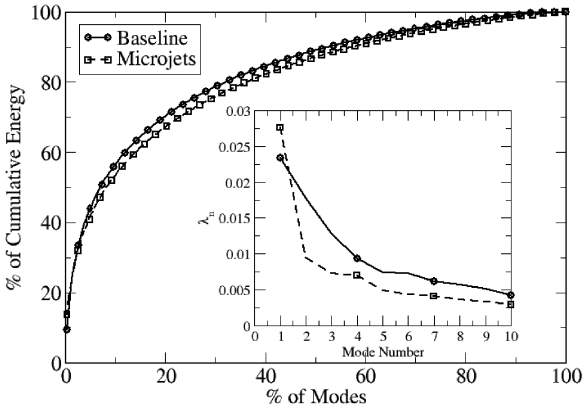

Fig. 16 Convergence of POD modes for pressure.

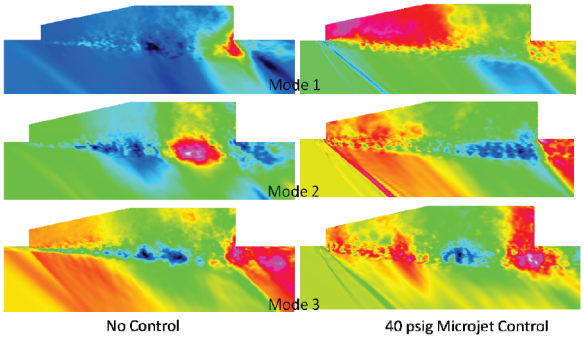

Fig. 17 POD modes of baseline vs control cases for pressure.

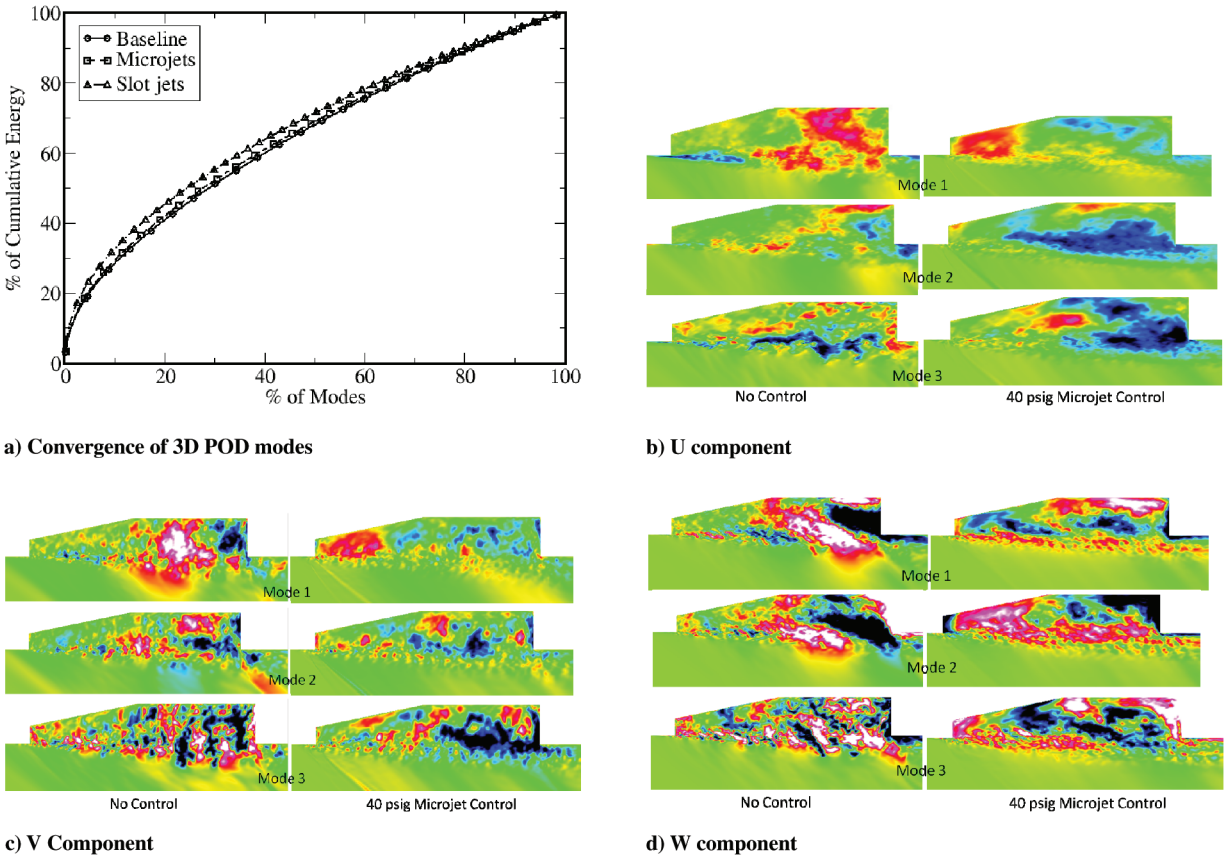

a) Convergence of 3D POD modes

b) U component

c) V Component

d) W component

Fig. 18 3-D POD modes using the entire flowfield data for the *u*, *v*, and *w* components.

demonstrate that it is important to include all components of the velocity field when analyzing the POD modes associated with such 3-D cavity flows.

V. Conclusions

Numerical simulations involving LES of supersonic flow over a nonrectangular cavity ($L/D = 5.6$) have been presented with control concepts that involve blowing through microjets and slot jets and a fence spoiler. The results from these simulations have been validated with experimental measurements of the surface pressures, and both show that there is an overall reduction of pressure fluctuations by 50% with the application of the leading-edge blowing concepts. The blowing concepts are seen to yield as good or better suppression of the fluctuating pressure levels compared with the spoiler, and, although the spoiler was not optimized, the blowing concepts are significantly more amenable to working at varying freestream conditions. Because of the fact that the mass/momentum of these concepts can be adjusted or tuned for different flow conditions, these are more efficient and practical than the spoiler concept.

The primary effect of the spoiler on the flowfield is seen to be the deflection of the shear layer. This alters the impingement of the shear layer on the aft end of the cavity, thereby modifying the feedback loop and effecting a reduction in the fluctuating pressure levels. Other than this, the effect on the evolution of turbulence in the shear layer itself is seen to be minimal.

The major effects of the blowing concepts are the changes in the structure of the turbulence in the shear layer over the cavity. The spanwise coherence of the shear layer (seen in the baseline case) is destroyed by the control jets leading to the creation of smaller vortical structures. The near-field turbulence production levels are enhanced by the action of the jets, but this is offset by a decrease in the length scale structures and, consequently, an increase in the dissipation levels. The characteristic flapping motion of the shear layer due to the spanwise coherence seen in the baseline case disappears, and in turn we see the smaller-scale vortical structures impinging on the aft wall. These structures have a smaller imprint on the wall pressure signature and cause the observed decrease in the unsteady pressure fluctuation levels. Looking at the mean and turbulence profiles of velocity and its components around the local vicinity of the cavity walls shows there are only slight differences between the baseline and control cases. Any significant increase in turbulence production is seen only the near field, whereas the slight increase in the shear layer thickness is seen to last the length of the cavity. Thus, the effect of control seems only to marginally affect the mean and turbulence quantities. The subtle yet significant changes it causes in the turbulence structure results in redistributing the energy from larger vortical structures in the baseline case to the smaller structures in the control cases and is what leads to the reduction in the fluctuating pressure levels on the cavity walls.

The POD modes of the velocity field in both 2-D (comprising a single plane and only U, V components) and 3-D, (of the whole cavity domain and including all components of velocity), and pressure field only in 2-D was presented for the baseline and microjet cases. The 2-D modes of velocity when compared with the experimental modes show reasonable qualitative agreement. These 2-D velocity modes appear to be very similar for the baseline and control case, which does not correlate well with the modes from the application to the pressure field. The pressure modes show that in the controlled case there is a redistribution of energy from the impinging event on the aft wall to structures further upstream in the cavity involving the interaction of the leading-edge separation bubble and the shear layer. The 3-D modes of velocity, on the other hand, which appear to be drastically different from the 2-D modes, correlate very well with the modes of pressure. Both the 3-D velocity modes and pressure modes point to redistribution of energy from the impinging event on the aft wall to recirculation structures upstream in the cavity. In addition, W component modes show smaller scale structure with control. Because the major effect of control is the change in spanwise structure of the shear layer, looking at a 2-D POD by neglecting the W component (especially for the control case) skews the physical insight of what the POD modes represent in terms of the actual

structure in the flowfield. The pressure field in the cavity is more or less 2-D in nature, and, hence, the 2-D POD of pressure can be a good representation of the flow.

Acknowledgments

The simulations presented here were carried out under funding provided through the AFRL/RBAI Separation Enhancement and Acoustic Reduction (SEAR) Program, James Grove, technical monitor. We would like to thank him for the many technical discussions and high performance computing computer time. The POD analysis carried out has been carried out under a Phase II SBIR award from AFRL/RB. Ryan Schmit was the contract monitor. Lawrence Ukeiley and George Shumway would also acknowledge partial support from an Air Force Office of Scientific Research program monitored by J. Schmisseur.

References

[1] Shaw, L., Bartel, H., and McAvoy, J., "Acoustic Environment in Large Enclosures With a Small Opening Exposed to Flow," *Journal of Aircraft*, Vol. 20, No. 3, March 1983, pp. 250–256. doi:10.2514/3.44860

[2] McGrath, S., and Shaw, L. L., "Active Control of Shallow Cavity Acoustic Resonance," AIAA Paper 96-1949, 1996.

[3] Rossiter, J. E., "Wind Tunnel Experiments on the Flow over Rectangular Cavities at Subsonic and Supersonic Speeds," Royal Aircraft Establishment, *Aeronautical Research Council Reports and Memoranda*, No. 3438, England, 1966.

[4] Heller, H. H., and Bliss, D. B., "Aerodynamically Induced Pressure Oscillations in Cavities-Physical Mechanisms and Suppression Concepts," Air Force Flight Dynamics Laboratory, Rept. TR-74-133, Wright–Patterson Air Force Base, OH, Feb. 1975.

[5] Shaw, L. L., Bartel, H., and McAvoy, J., "Prediction and Suppression of the Acoustic Environment in Large Enclosures With a Small Opening Exposed to Aerodynamic Flow," AIAA Paper 82-0121, 1982.

[6] Sarno, R. L., and Franke, M. E., "Suppression of Flow-Induced Pressure Oscillations in Cavities," *Journal of Aircraft*, Vol. 31, No. 1, Feb. 1994, pp. 90–96. doi:10.2514/3.46459

[7] Smith, D. L., and Shaw, L. L., "Prediction of the Pressure Oscillation in Cavities Exposed to Aerodynamic Flow," Air Force Flight Dynamics Laboratory, Rept. TR-75-34, Wright–Patterson Air Force Base, OH, Oct. 1975.

[8] Cattafesta, L., Williams, D., Rowley, C., and Alvi, F., "Review of Active Control of Flow-Induced Cavity Resonance," AIAA Paper 2003-3567, 2003.

[9] Rowley, C. W., and Williams, D. R., "Dynamics and Control of High Reynolds Number Flows over Open Cavities," *Annual Review of Fluid Mechanics*, Vol. 38, Jan. 2006, pp. 251–276. doi:10.1146/annurev.fluid.38.050304.092057

[10] Zhuang, N., Alvi, F. S., Alkislar, B., and Shih, C., "Supersonic Cavity Flows and Their Control," *AIAA Journal*, Vol. 44, No. 9, 2006, pp. 2118–2128. doi:10.2514/1.14879

[11] Zhuang, N., Alvi, F. S., and Shih, C., "Another Look at Supersonic Cavity Flows and Their Control," AIAA Paper 2005-2803, 2005.

[12] Arunajatesan, S., Kannepalli, C., and Sinha, N., "Analysis of Control Concepts for Cavity Flows," *12th AIAA/CEAS Aeroacoustics Conference*, AIAA Paper 2006-2427, 2006.

[13] Ukeiley, L. S., Sheehan, M., Coiffet, F., Alvi, F. S., Arunajatesan, S., and Jansen, B., "Control of Pressure Loads in Geometrically Complex Cavities," *Journal of Aircraft*, Vol. 45, No. 3, 2008, pp. 1014–1024. doi:10.2514/1.33324

[14] Sheehan, M. V., "Supersonic Flow and its Control over Highly Three Dimensional Cavities," Ph.D. Dissertation, Florida State Univ., Tallahassee, FL, 2007.

[15] Shipman, J. D., Arunajatesan, S., Cavallo, P. A., Sinha, N., Ukeiley, L., and Alvi, F., "Flow Control for Enhanced Store Separation," *45th Aerospace Sciences Meeting and Exhibit*, AIAA Paper 2007-1236, Jan. 2007.

[16] Bauer, R., and Dix, R., "Engineering Model of Unsteady Flow in a Cavity," Arnold Engineering Development Center, Rept. 91-17, Tullahoma, TN, Dec. 1991.

[17] Rai, M. M., and Moin, P., "Direct Numerical Simulation of Transition and Turbulence in Spatially Evolving Boundary Layer," *Journal of Computational Physics*, Vol. 109, 1993, pp. 162–192.

[18] Rai, M. M., "Navier–Stokes Simulations of Blade Vortex Interaction Using High-Order Accurate Upwind Schemes," *25th Aerospace Sciences Meeting*, AIAA Paper 87-0543, Jan. 1987.

[19] Menon, S., "Active Control of Combustion Instability in a Ramjet Using Large Eddy Simulations," *29th AIAA Aerospace Sciences Meeting*, AIAA Paper 91-0411, 1991.

[20] Arunajatesan, S. A., and Dash, S. M., "Progress Towards Hybrid RANS-LES Modeling for High-Speed Jet Flows," *40th AIAA Aerospace Sciences Meeting and Exhibit*, AIAA Paper AIAA-2002-0428, Jan. 2002.

[21] Ayyalasomayajula, H., Arunajatesan, S., Kannepalli, C., and Sinha, N., "Large Eddy Simulation of a Supersonic Flow Over a Backward-Facing Step for Aero-Optical Analysis," *44th Aerospace Sciences Meeting and Exhibit*, AIAA Paper AIAA-2006-1416, Jan. 2006.

[22] Nichols, R., "Comparison of Hybrid Turbulence Models for a Circular Cylinder and a Cavity," *AIAA Journal*, Vol. 44, No. 6, June 2006, pp. 1207–1219. doi:10.2514/1.17016

[23] Heller, H. H., and Bliss, D. B., "The Physical Mechanism of Flow Induced Pressure Fluctuations in Cavities and Concepts for Suppression," AIAA Paper 75-491, March 1975.

[24] Ukeiley, L. S., Ponton, M. K., Seiner, J. M., and Jansen, B., "Suppression of Pressure Loads in Cavity Flows," *AIAA Journal,*, Vol. 42, No. 1, 2004, pp. 70–79.

[25] Lumley, J. L., "The Structure of Inhomogeneous Turbulent Flow," *Atmospheric Turbulence and Radio Wave Propagation*, edited by A. M. Yaglom and V. I. Tatarski, Nauka, Moscow, 1967, pp. 166–178.

[26] Holmes, P., Lumley, J., and Berkooz, G., *Turbulence, Coherent Structures, Dynamical Systems and Symmetry*," Cambridge Univ. Press, Cambridge, U.K., 1998.

[27] Sirovich, L., "Turbulence and the Dynamics of Coherent Structures. Part 1: Coherent Structures," *Quarterly of Applied Mathematics*, Vol. 45, No. 3, 1987, pp. 561–571.

[28] Shumway, G., Sheehan, M., Alvi, F., and Ukeiley, L., "Flow Structure of Supersonic Cavity Flow With and Without Control," *Bulletin of the American Physical Society*, Vol. 52, No. 17, Nov. 2007, p. 289.

[29] Wanstrom, M., George, W. K., and Meyer, K. E., "Stereoscopic PIV and POD Applied to the Fare Turbulent Axisymmetric Jet," AIAA Paper 2006-3368, 2006.

M. Glauser
Associate Editor